Articles in PresS. Am J Physiol Lung Cell Mol Physiol (August 15, 2014). doi:10.1152/ajplung.00092.2014

Cigarette smoke-induced iBALT mediates macrophage activation in a B cell-dependent manner in COPD

Gerrit John-Schuster[1,¶], Katrin Hager[1,¶], Thomas M. Conlon[1], Martin Irmler[2], Johannes Beckers[2,,3], Oliver Eickelberg[1,4], and Ali Önder Yildirim[1, *]

[1]Comprehensive Pneumology Center, Institute of Lung Biology and Disease
Helmholtz Zentrum München, Member of the German Center for Lung Research
Ingolstädter Landstr. 1, 85764 Neuherberg, Germany

[2]Institute of Experimental Genetics, Helmholtz Zentrum Muenchen, Ingolstädter Landstr. 1, 85764 Neuherberg, Germany

[3]Technical University Munich, Chair of Experimental Genetics, Am Hochanger 8, 85350 Freising-Weihenstephan, Germany

[4]Klinikum der Universität München, Max-Lebsche-Platz 31, 81377 München

[¶]Equal contribution

Running head: B cell deficiency protects against COPD

Key words: COPD, B cells, iBALT, IL-10, macrophages

Corresponding author: Ali Önder Yildirim, Tel +49-89-3187-4037; Fax +49-89-3187-2400
oender.yildirim@helmholtz-muenchen.de

Abbreviations

CS, cigarette smoke; FA, filtered air; LF, lymphoid follicle; TLO, tertiary lymphoid organ; iBALT, inducible bronchus-associated lymphoid tissue; BAL, bronchoalveolar lavage; KC, keratinocyte chemoattractant; TNF-α, tumor necrosis factor α; MIP2, macrophage inflammatory protein 2-alpha; MIG, monokine induced by interferon-γ; MMP12, matrix metalloproteinase 12; NE, neutrophil elastase; GM-CSF, granulocyte macrophage colony-stimulating factor; CO, carbon monoxide; CO-Hb, carboxyhemoglobin; TPM, total particulate matter.

Abstract

Chronic obstructive pulmonary disease (COPD) is characterized by a progressive decline in lung function, caused by exposure to exogenous particles, mainly cigarette smoke (CS). COPD is initiated and perpetuated by an abnormal CS-induced inflammatory response of the lungs, involving both innate and adaptive immunity. Specifically, B cells organized in iBALT structures and macrophages accumulate in the lungs and contribute to CS-induced emphysema, but the mechanisms thereof remain unclear. Here, we demonstrate that B cell-deficient mice are significantly protected against CS-induced emphysema. Chronic CS exposure led to an increased size and number of iBALT structures, and increased lung compliance and mean linear chord length in WT, but not B cell-deficient mice. The increased accumulation of lung resident macrophages around iBALT and in emphysematous alveolar areas in CS-exposed WT mice coincided with upregulated MMP12 expression. *In vitro* co-culture experiments using B cells and macrophages demonstrated that B cell-derived IL-10 drives macrophage activation and MMP12 upregulation, which could be inhibited by an anti-IL10 antibody. In summary, B cell function in iBALT formation seems necessary for macrophage activation and tissue destruction in CS-induced emphysema, and possibly provides a new target for therapeutic intervention in COPD.

Introduction

Chronic obstructive pulmonary disease (COPD) is a major public health problem and its prevalence as well as morbidity and mortality are still rising worldwide (50, 53). The stimulus of long-term exposure to toxic gases and particles, most often cigarette smoke (CS) induces mucus production, remodeling of small airways, septal tissue damage and chronic bronchitis (36). These severe pathophysiological changes are the cause for the constant and accelerated decline in lung function observed in patients suffering from COPD. Currently, there is no therapy for COPD and treatment can only aim at alleviating symptoms.

In the lung, chronic CS exposure causes activation and influx of various inflammatory cells, including both innate immune cells, with macrophages and neutrophils predominating, and adaptive immune cells, specifically T and B lymphocytes (2, 20). Their numbers are increased in both airways and parenchyma of patients with COPD (4, 44, 45). Moreover, the progression and severity of COPD are associated with increasing infiltration of the airways by innate and adaptive immune cells, which form ectopic lymphoid follicles (LFs) consisting of B cells surrounded mainly by CD4 T cells (21). Further studies have confirmed that increased B cell numbers are observed in the mucosa of large airways in COPD patients compared to controls (16) and the number of B cell follicles present in the lung also increases with disease severity (52).

Highly organized ectopic LFs are referred to as tertiary lymphoid organs (TLOs) because of their structural similarity to secondary lymphoid organs, which includes distinct B and T cell areas, germinal centers and high endothelial venules (1, 10, 33). TLOs form in various tissues targeted by chronic inflammation and have an important role in maintaining immune responses that can either be harmful or beneficial. They have been associated with local pathogenic autoantibody production (37, 42) or, in respiratory infections and lung cancer,

with favorable outcome (14, 17, 34). However, it is still under critical debate whether TLOs in COPD are beneficial or harmful because their role in COPD pathogenesis remains unknown (8, 57).

Lung TLOs, preferentially termed inducible bronchus-associated lymphoid tissue (iBALT), have also been described in *in vivo* models of COPD. Mice develop LFs after chronic CS exposure (12, 52). Recently, Litsiou *et al.* discovered that CXCL13 is involved in lymphoid neogenesis in COPD by promoting B cell migration to ectopic sites of lymphoid tissue formation and by upregulating lymphotoxin on B cells, which in turn further induces CXCL13 required for follicle expansion (29). In CS-exposed mice, administration of an anti-CXCL13 antibody prevents the formation of pulmonary LFs thereby attenuating the destruction of alveolar walls and BAL inflammation (6).

Aside from their involvement in lymphoid neogenesis and their antibody-producing capacity, B cells can also function as antigen-presenting cells and provide co-stimulatory signals to T cells (15). Furthermore, the secretion of a variety of cytokines including IL-6 and IL-10 may enable B cells to influence and modulate differentiation and polarization of macrophages, T cells and dendritic cells during the development of the immune response thereby regulating immune reactions (23). B cell-mediated modulation of macrophage effector functions via cytokine secretion has been described to be important for the outcome of various models of infection, inflammation and cancer (3, 32, 56).

In COPD, the role of innate immune cells in CS-induced lung inflammation and subsequent emphysema development has been addressed in several animal studies (5, 12). Macrophage-derived matrix metalloproteinase (MMP) 12 was described as being required for the induction of experimental emphysema after prolonged CS exposure because CS-exposed MMP12 knockout mice failed to recruit macrophages and did not develop lung destruction (7, 18).

This finding points to a primary role for macrophages and derived factors in the development of emphysema both in patients and CS-exposed animals. We hypothesized that B cell-dependent iBALT formation is involved in macrophage activation and polarization thereby inducing and maintaining a severe inflammatory response that is driving the pathophysiological changes in COPD. Therefore, we monitored the development of COPD in wildtype (WT) and B cell-deficient knockout mice exposed to CS. We characterized structural and functional changes, iBALT formation and the inflammatory response occurring in lung tissue. Interestingly, we identified B cell-derived IL-10 as one of the possible key regulators of MMP12 production in macrophages. Thus, the responsiveness of B cells to CS induces iBALT formation in the lung thereby leading to accumulation and activation of matrix-degrading macrophages. This finding could lead to the development of new therapeutic targets for the treatment of COPD patients.

Materials and Methods

Animals and maintenance

B cell deficient B6.129S2-Igh-6^{tm1Cgn} mice (27), also known as μMT mice and their respective eight to ten weeks old pathogen-free female C57BL/6 WT control mice were purchased from Charles River (Sulzfeld, Germany). Animals were housed in rooms maintained at constant temperature and humidity with a 12 hour light cycle and were allowed food and water *ad libitum*. All experiments were conducted under strict governmental and international guidelines and were approved by the local government for the administrative region of Upper Bavaria.

Cigarette smoke (CS) exposure

Cigarette smoke (CS) was generated from 3R4F Research Cigarettes (Tobacco Research Institute, University of Kentucky, Lexington, KY). Mice were whole body exposed to active, i.e. 100% mainstream CS of 500 mg/m^3 total particulate matter (TPM) for 50 min twice per day for 1, 4 and 6 months in a manner mimicking natural human smoking habits (24). Control mice were kept in a filtered air (FA) environment, but exposed to the same stress as CS-exposed animals. 24 h after the last CS exposure, mice were sacrificed.

The TPM level was monitored via gravimetric analysis of quartz fiber filters prior and after sampling air from the exposure chamber and measuring the total air volume. CO concentrations in the exposure chamber were constantly monitored by using a GCO 100 CO Meter (Greisinger Electronic, Regenstauf, Germany) and reached values of 288± 74 ppm. All mice tolerated CS-mediated CO concentrations without any sign of toxicity, with CO-Hb levels of 12.2 ± 2.4%. Experiments were performed with n=8 animals per group and were repeated twice. All animals were subjected to lung function analysis. Afterwards, n=4 animals

per group were lavaged, the right lung was shock-frozen in liquid nitrogen and the left lung was fixed in paraformaldehyde (PFA; see below). The remaining n=4 animals per group were used for FACS analysis of whole lung single-cell suspensions (see below).

Elastase application

Emphysema was induced in mice by oropharyngeal application of porcine pancreatic elastase (PPE, 80 U/kg body weight in 80 µl volume) as previously described (59). Control mice received 80 µl of sterile PBS. Mice were killed on day 28. Experiments were performed with n=8 animals per group and were repeated twice.

Lung function measurement

Pulmonary function in mice was measured using a flexiVent system (Scireq, Montréal, Canada). Mice were anesthetized with ketamine-xylazine, tracheostomized and connected to the flexiVent system. Mice were ventilated with a tidal volume of 10 ml/kg at a frequency of 150 breaths/min in order to reach a mean lung volume similar to that of spontaneous breathing. Testing of lung mechanical properties including dynamic lung compliance and resistance was carried out by a software-generated script. Measurements were repeated four times per animal.

Preparation of bronchoalveolar lavage (BAL)

BAL was obtained to perform total and differential cell counts for inflammatory cell recruitment of neutrophils, macrophages and lymphocytes. The lungs were lavaged by instilling the lungs with 4 x 0.5 ml aliquots of sterile PBS (Gibco, Life Technologies,

Darmstadt, Germany). For cytospins, cells were spun down at 400 g and re-suspended in RPMI-1640 medium containing 10% FCS (both from Gibco). Total cell counts were determined in a hemocytometer. Differential cell counts were performed using morphological criteria on May-Grünwald-Giemsa-stained cytospins (200 cells/ sample). BAL fluid was used to evaluate cytokine secretion via multiplex analysis.

Lung tissue processing

Lung tissue was either shock-frozen in liquid nitrogen to isolate mRNA for gene expression analysis or fixed at a constant pressure (20 cm fluid column) by intratracheal instillation of PBS buffered 6% paraformaldehyde (PFA) and embedded into paraffin for histological analysis of hematoxylin-eosin (HE)-stained slides and for immunohistochemistry.

For analysis of lymphocyte infiltration, single-cell suspensions of whole lung tissue were used. Lungs were perfused with sterile PBS via the right ventricle to clear leukocytes and erythrocytes from the pulmonary circulation. Lung homogenization was performed via enzymatic digestion and mechanical dissociation steps using a lung dissociation buffer and the gentleMACS Dissociator (both from Miltenyi Biotec, Bergisch Gladbach, Germany). After dissociation, samples were applied to a filter to remove any remaining larger particles from the single-cell suspensions.

FACS analysis of whole lung lymphocyte infiltration

For FACS analysis of single-cell suspensions, one part of the sample was directly labeled with FACS antibodies against T and B cell surface antigens. Staining of activated T lymphocytes was performed with antibodies against CD4, CD8 (both from eBioscience, San Diego, CA)

and B lymphocytes were stained with an antibody against CD20 (eBioscience). Remaining lung cells were subjected to density gradient centrifugation using Pancoll (PAN Biotech, Aidenbach, Germany) to isolate mononuclear cells. Isolated cells were cultured over night in anti-CD3/anti-CD28-coated plates to perform intracellular cytokine staining. On the following day, cultivated cells were restimulated with leukocyte activation cocktail with Golgi Plug (BD Pharmingen) for 4h. Afterwards, cells were stained with anti-CD4, fixed in 2% formaldehyde, permeabilized in 0.3% saponin buffer and stained with antibodies against IL-17A, IFN-γ (both from eBioscience) and IL-4 (Biozol) to distinguish between different T helper cell subpopulations. Multicolor analysis of stained cells was conducted with a BD FACSCanto II flow cytometer (BD Biosciences, Heidelberg, Germany) and BD FACSDiva software.

Quantitative morphometry

Design-based stereology was used to analyze sections using an Olympus BX51 light microscope equipped with a computer-assisted stereological toolbox (newCAST, Visiopharm, Hoersholm, Denmark) on HE-stained lung tissue slides as previously described (59). Air space enlargement was assessed by quantifying mean linear chord length (MLI) on 30 fields of view per lung. Briefly, a line grid was superimposed on lung section images. Intercepts of lines with alveolar septa and points hitting air space were counted to calculate MLI applying the formula $MLI = \sum P_{air} \times L(p) / \sum I_{septa} \times 0{,}5$. P_{air} are the points of the grid hitting air spaces, L(p) is the line length per point, I_{septa} is the sum of intercepts of alveolar septa with grid lines.

Volume of inducible bronchus-associated lymphoid tissue (iBALT) normalized to the basal membrane was quantified on 50 fields of view per lung by counting points hitting iBALT (P_{iBALT}) and intercepts of lines with vessels and airways ($I_{airway+vessel}$). The volume was calculated by applying the formula $V/S = \sum P_{iBALT.} \times L(p) / \sum I_{airway+vessel}$.

The frequency of macrophages expressing MMP12 in lung tissue was quantified on 30 fields of view per lung. A frame grid was superimposed on lung section images. Within the frame, macrophages either positive or negative for MMP12 staining were counted and the percentage of MMP12-positive macrophages was calculated.

Immunohistochemistry

For immunohistochemistry, lungs were fixed in paraformaldehyde and embedded into paraffin. After deparaffinizing in xylene and rehydrating in alcohol, the tissue was treated with 1.8% (v/v) H_2O_2 solution (Sigma-Aldrich, St. Louis, MO) to block endogenous peroxidase. Heat induced epitope retrieval was performed in HIER Citrate Buffer (pH 6.0, Zytomed Systems) in a Decloaking chamber (Biocare Medical, Concord, CA). To inhibit nonspecific binding of antibodies, tissue slides were treated with a rodent blocking antibody (Biocare Medical). After overnight incubation with primary antibodies against MMP12 (Abcam, Cambridge, UK), CD45R (BD Pharmingen), CD3 (Sigma Aldrich) or IL-10 (Santa Cruz Biotechnology, Dallas, TX), tissue slides were incubated with an alkaline phosphatase-labeled secondary antibody (Biocare Medical). Signals were amplified by adding chromogen substrate Vulcan fast red (Biocare Medical). Slides were counterstained with hematoxylin (Sigma-Aldrich) and dehydrated in xylene. Afterwards, coverslips were mounted.

Quantitative real time RT-PCR

Total RNA from lung tissue homogenate was isolated using a peqGOLD Total RNA Kit (Peqlab, Erlangen, Germany) according to the manufacturer's instructions. cDNA was synthesized using Random Hexamers and MuLV Reverse Transcriptase (Applied Biosystems,

Darmstadt, Germany). mRNA expression of target genes KC (CXCL1), TNF-α, MCP1, MMP12, TIMP1, F4/80, IL-17A, CXCL13, IL-10, IL-6 and GM-CSF in comparison to housekeeping control hypoxanthine-guanine phosphoribosyltransferase (HPRT)-1 was determined using Platinum SYBR Green qPCR SuperMix (Applied Biosystems) on a StepOnePlus™ 96 well Real-Time PCR System (Applied Biosystems, Carlsbad, CA). Relative transcript expression of a gene is given as $2^{-\Delta CT}$ ($\Delta Ct = Ct_{target} - Ct_{reference}$), relative changes compared to control are $2^{-\Delta\Delta Ct}$ values ($\Delta\Delta Ct = \Delta Ct_{treated} - \Delta Ct_{control}$). Primers were generated using Primer-BLAST software (58) and according to published mRNA sequences.

Western blot

20 µg of protein was separated by SDS-PAGE, transferred onto a polyvinylidene difluoride membrane (Bio-Rad, Munich, Germany), blocked by 5% non-fat milk and immunoblotted with anti-MMP12 (Millipore, Schwalbach, Germany) antibody. Upon developing with Amersham ECL Prime reagent (GE Healthcare, Freiburg, Germany) the bands were detected and quantified using the Chemidoc XRS system (Bio-Rad).

Multiplex cytokine analysis

Concentrations of secreted cytokines and chemokines KC (CXCL1), TNF-α and MCP1 in BAL were determined using a magnetic bead-based MILLIPLEX *MAG* multiplex assay (Millipore, Schwalbach, Germany) and analyzed on a Luminex^{100} (Bio-Rad). For this assay, BAL fluid was concentrated (10x) by ultrafiltration in Amicon Ultra-0.5 centrifugal filter devices (Millipore).

In vitro cell culture experiments

In vitro experiments were performed with the B cell lymphoma line A20 and the macrophage cell line MH-S, both maintained at 37°C in 5% CO_2 atmosphere. A20 cells were cultured in RPMI-1640 supplemented with 10% FCS, 0.1 mM 2-mercaptoethanol, 100 U/ml penicillin-streptomycin, 10mM Hepes, 2mM L-glutamin, 1mM sodium-pyruvat, 0.1mM non-essential amino acids, and 1x MEM vitamin solution. MH-S cells were maintained in RPMI-1640 supplemented with 10% FCS and 0.05 mM 2-mercaptoethanol.

CS extract for stimulation of cells was prepared by bubbling smoke from 3 research cigarettes (3R4F; see above) through 30 ml of RPMI-1640 cell culture medium at puffing speed in a closed environment with limited air flow. This stock was considered as 100% CS extract.

For testing the influence of B cell secreted cytokines on macrophages, A20 cells were stimulated either with LPS or with CS extract for 24 h and afterwards, supernatants were used for stimulation of MH-S cells. In brief, A20 cells were seeded at a density of $4x10^5$ cells per well in a 24 well plate. The following day, A20 cells were stimulated either with LPS [20 µg/ml] as positive control or with CS extract [1%] and [4%] for 24 h. Pure cell culture medium served as negative control. After 24 h, supernatants from A20 cells were removed, centrifuged and used for stimulation of MH-S cells that had been seeded the day before at a density of $2x10^5$ cells per well in a 24 well plate. Stimulation was performed for 6 h; afterwards, cells were lysed for subsequent RNA isolation. Blockade of IL-10 signaling was performed by adding a blocking anti-IL-10 antibody (Santa Cruz Biotechnology) to the supernatants 30 min before stimulation of MH-S cells. All treatments did not significantly affect cell viability (data not shown).

Determination of IL-10 secretion by ELISA

Concentrations of IL-10 in the cell culture supernatants were determined by a commercially available kit for enzyme-linked immunosorbent assay (eBioscience), and normalized to the protein concentration of the lysed cells (as measured by BCA Protein Assay).

Th17 cell differentiation

Naive CD4 T cells were purified from total murine splenocytes using the CD4+CD62L+ T cell Isolation Kit II (Miltenyi Biotec). These were then stimulated for 72 h with anti-CD3/anti-CD28 coupled beads (Life Technologies, Darmstadt, Germany), along with recombinant human TGFβ (10 ng/ml, R&D Systems, Wiesbaden, Germany), IL-6 (60 ng/ml, R&D Systems), anti-IL-4 (10 ng/ml, BioLegend, San Diego, CA), anti-IL-12 (10 ng/ml, BioLegend), anti-IFN-γ (5 ng/ml, BioLegend) and anti-IL-2 (2.5 ng/ml, Miltenyi Biotec). Th0 control cells were stimulated with anti-CD3/anti-CD28 coupled beads alone for 72 h.

Cells were restimulated with PMA (20nM) and Ionomycin (1μM, both from Merck, Darmstadt, Germany) for 5 h with the addition of Brefeldin A (10 μg/ml, Sigma-Aldrich) for the last 2.5 h. Cells were stained with anti-mouse CD4 and Fixable Viability Dye eFluor 450 (both from eBioscience) before fixation with 4% PFA and permeabilization in PBS/0.5% Saponin/ 1%BSA. Cells were then stained with anti-IL-17A (eBioscience) before being analyzed on a BD FACSCanto II flow cytometer (BD Biosciences).

Microarray analysis

Lung tissue was obtained from CS-treated C57BL/6 mice (n=3) and FA-treated control animals (n=3) as described above. Total RNA was isolated employing the RNeasy Mini Kit

297 (Qiagen) including digestion of remaining genomic DNA. The Agilent 2100 Bioanalyzer was
298 used to assess RNA quality and only high quality RNA (RIN>7) was used for microarray
299 analysis. 300 ng of total RNA were amplified using the Illumina TotalPrep RNA
300 Amplification kit (Ambion). Amplified cRNA was hybridized to Mouse Ref-8 v2.0
301 Expression BeadChips (Illumina, San Diego, CA). Staining and scanning were done
302 according to the Illumina expression protocol. Data was processed using the
303 GenomeStudioV2010.1 software (gene expression module version 1.6.0) in combination with
304 the MouseRef-8_V2_0_R3_11278551_A.bgx annotation file. The background subtraction
305 option was used and an offset to remove remaining negative expression values was
306 introduced. CARMAweb was used for quantile normalization (40). Statistical analyses were
307 performed by utilizing the statistical programming environment R (R Development Core
308 Team, (48)) implemented in CARMAweb. Genewise testing for differential expression was
309 done employing the limma t-test and Benjamini-Hochberg multiple testing correction (FDR <
310 10%). Pathway enrichment analyses were done with Ingenuity Pathway Software and
311 significant terms ($p<0.05$) were determined. Microarray data was submitted to GEO and link
312 for review was generated:
313 http://www.ncbi.nlm.nih.gov/geo/query/acc.cgi?token=etknuseghzkfvkn&acc=GSE52509

314

315 *Statistics*

316 Results are given as mean values ± SD. One-way ANOVA following Bonferroni post test was
317 used for all studies with more than two groups. Analyses were conducted using GraphPad
318 Prism 6 software (GraphPad Software, La Jolla, CA).

319

Results

B cells are required for inducible bronchus-associated lymphoid tissue (iBALT) formation after CS exposure.

In the lungs of severe COPD patients, increased T and B cell numbers and lymphoid follicle (LF)-like structures have been described (21, 29). To investigate the role of B cells in a CS-induced COPD mouse model, B cell deficient (μMT) and WT mice were exposed to CS for one to six months. We found that in WT animals marginal inflammatory cell infiltrates could be seen after one month of CS exposure compared to FA control mice. After 4 and 6 months of CS exposure, these infiltrates forming in WT mice, which we termed iBALT, showed significant increases in volume as shown by quantitative morphological assessment (Figure 1A, B). Interestingly, the formation of iBALTs did not proceed in the lungs of μMT mice exposed to CS. Previously, Litsiou *et al.* have shown that CXCL13 plays an important role in LF formation (29). Therefore, we investigated whether B cell deficiency *in vivo* leads to altered CXCL13 expression. Using qPCR analysis we found a significant induction of CXCL13 mRNA expression in WT mice compared to μMT mice supporting the finding of iBALT formation in WT mouse lungs only (Figure 1C).

We further investigated the immune cell composition of iBALT structures by staining for B and T lymphocytes. CS-induced follicles in WT mice contained an abundance of CD45R-positive B cells and CD3-positive T cells compared to FA control and μMT mice (Figure 1D, E). Nevertheless, we observed slightly increased numbers of CD3-positive T cells in μMT lungs after CS exposure.

These expected results demonstrate that in our clinically relevant COPD mouse model B cells play crucial roles in CS-induced formation of iBALT structures, which predominantly consist of B and T cells in WT mice.

B cell deficient mice show different lymphocyte infiltration in lung tissue after chronic CS exposure.

Based on the clear differences in lung tissue inflammation and iBALT formation in WT mice after CS exposure (Figure 1), we aimed at confirming our lung tissue results by using flow cytometric quantification of B cells and CD4-positive T cell subsets in single-cell suspensions of whole lungs from WT and µMT mice. Compared to FA animals, lungs from CS-exposed WT mice revealed increased numbers of CD20-positive B cells starting from one month of exposure (Figure 2A). Numbers of CD4-positive T cell subtypes Th1 and Th2 increased during the whole time course, but - except for lower Th1 cell numbers at 6 months in CS-exposed µMT compared to WT mice - no significant differences were observed for CS exposure and between WT and µMT mice, respectively (Figure 2C, D). Th17 cell numbers were significantly different after six months of CS exposure in WT mice when compared to CS-exposed µMT and FA mice (Figure 2E). This was supported by significantly elevated IL-17 mRNA levels at the later time point of six months (Figure 2F). Recently, T helper cell subsets have been further characterized by dual expression of the prototypic cytokines. Therefore, we undertook a more detailed analysis of the subsets found in our CS-exposed mice. We did not observe an increase in IFN-γ^+ Th17, IL-17^+ Th2 and IFN-γ^+IL-17^+IL-4^+ cells after CS exposure for one and four months. After CS exposure for six months, these subsets were significantly increased in WT compared to FA and CS-exposed µMT mice (IFN-γ^+ Th17: 2.8 ± 1.3% in WT vs. 1.4 ± 1.0% in µMT mice; IL17^+ Th2: 0.6 ± 0.2% in WT vs. 0.2 ± 0.1% in µMT mice; IFN-γ^+IL-17^+IL-4^+: 0.5 ± 0.3% in WT vs. 0.1 ± 0.1% in µMT mice).

Because we did not observe increases in Th17 cells after CS exposure of µMT mice, we investigated whether B cell deficiency alters the ability of CD4 T cells to differentiate into Th17 cells in these animals. We found that there was no differentiation defect in µMT mice as

368 indicated by comparable Th17 levels after *ex vivo* stimulation of naïve CD4 T cells from WT
369 and μMT mice (12.5 ± 2.0% vs. 14.1 ± 3.0% Th17 cells).

370 These results demonstrate that chronic CS exposure is associated with early increases in B
371 cells and later increases of Th17 cells in lung tissue of WT mice.

372

373 ***B cells play a critical role in CS-induced emphysema development.***

374 CS-induced lung damage was assessed by lung function analysis and by determining mean
375 linear chord length (MLI) using the computer-assisted stereological toolbox. After one month
376 of chronic CS exposure, significant changes in lung architecture and lung compliance could
377 neither be detected for WT nor for μMT mice compared to the respective FA control animals
378 (Figure 3). However, there was a significant increase in emphysema development after four
379 months of exposure to CS in the lungs of WT mice when compared to CS-exposed μMT and
380 FA mice. We further exposed WT and μMT animals to CS for another two months to enhance
381 the CS-induced emphysema response. Interestingly, there were no changes in MLI in μMT
382 animals even after six months of exposure to CS compared to FA control groups (Figure 3A,
383 B). Lung compliance was further augmented in WT compared with μMT mice exposed to CS
384 for 4 and 6 months (Figure 3C). In contrast, slight age-dependent increases in lung
385 compliance and MLI were observed for both WT and μMT mice during the whole time
386 course. These data were confirmed by a reduction of body weight in CS-exposed WT mice,
387 whereas both μMT groups showed comparable body weight levels (Figure 3D). These results
388 indicate that μMT mice were protected against CS-induced airspace enlargement.

389 To rule out the possibility that μMT mouse lungs are generally protected against airspace
390 enlargement as shown by Lucey *et al.* for combined TNF-α- and IL-1βR-deficient mice (30),
391 as well as to clarify the role of immune cells, specifically B cells in emphysema development

we treated μMT mice with porcine pancreatic elastase (PPE). In the elastase mouse model, emphysema develops independent of immune cell (re)actions. Interestingly, oropharyngeal administration of elastase resulted in severe pulmonary emphysema after 28 days in both WT and μMT mice as demonstrated by HE-stained lung tissue slides (Figure 4A). Quantitative morphological assessment confirmed airspace enlargement as indicated by significant increases in MLI for both groups (Figure 4B). The emphysematous changes in WT and μMT animals were associated with significantly increased lung compliance (Figure 4C). As expected, HE-stained lung sections did not show any significant tissue inflammation in the lungs of elastase-exposed WT and μMT mice (Figure 4A).

Our observations indicate that time-dependent iBALT formation and expansion in WT mice after CS exposure are also associated with the development of COPD.

iBALT induces macrophage activation and polarization.

Since B cells and iBALT appear to be crucial for the development of CS-induced emphysema, and macrophage-derived MMP12 was described as being required for the induction of experimental emphysema after prolonged CS exposure (18), the role of B cells in accumulation and activation of tissue macrophages in the chronic model was investigated. Despite the lack of iBALT formation in μMT mice after chronic CS exposure (Figure 1) we did not observe any differences in secreted BAL cytokine and tissue mRNA expression levels for TNF-α, KC and MCP1 in both CS-exposed groups (Figure 5A, B). This was possibly due to similar CS-induced inflammatory reactions by lung epithelial cells. The comparable levels of BAL cytokines and tissue mRNA expression were confirmed by similar increases in total BAL inflammatory cell counts in CS-exposed WT and μMT mice . For both groups, a significant and comparable increase in total cells counts in CS-exposed mice compared to FA

controls was observed at all-time points (fold increase compared to FA after 6 months CS exposure: 5.0 ± 1.0 in WT vs. 4.2 ± 1.3 in μMT mice).

However, in the lung tissue of WT animals, we observed significantly increased numbers of MMP12-stained macrophages located especially in iBALT as well as in the emphysematous alveolar lumen (Figure 6A). μMT mice on the other hand showed significantly lower staining for MMP12, which is consistent with the data obtained for reduced iBALT formation after CS exposure in these animals. Interestingly, we observed staining for MMP12 in airway epithelial cells in μMT mice. Quantitative analysis of MMP12 expressing macrophage numbers in lung tissue also revealed significantly higher values for CS-exposed WT compared to μMT mice (Figure 6B).

We further investigated mRNA expression levels for the macrophage marker F4/80. We noticed increases in F4/80 mRNA expression after CS exposure for both WT and μMT mice, but levels were significantly higher in WT mice at 4 and 6 months of exposure (Figure 6C), indicating higher macrophage accumulation in WT lung tissue. This was confirmed by qPCR for MMP12, which showed strong CS-induced increases for WT and μMT mice, but also significantly higher expression for WT animals at 4 and 6 months of exposure (Figure 6D). The stronger increase in MMP12 expression in WT mice further led to a higher MMP12/TIMP1 ratio in those animals, indicating a disturbed balance of MMP12 and its inhibitor TIMP1 (Figure 6E). Furthermore, western blot analysis for MMP12 using whole lung tissue lysates from WT and μMT mice after 6 months of CS revealed a significant increase in active protein in CS-exposed WT compared to μMT mice (Figure 6F). Because MMP12 is considered a marker for M2 macrophages polarization, we also analyzed the gene expression profile of several M1 and M2 markers. We did not observe increases in gene expression for the M1 markers iNOS and IL-6 after CS exposure in both WT and μMT

animals (Figure 6G). In contrast, besides MMP12 M2 markers FIZZ1 and Mrc1 were elevated in WT mice starting from 4 months of CS exposure. These data strongly indicate that CS-induced iBALT is involved in macrophage activation and positioning.

B cell-derived IL10 activates macrophages.

To decipher the genes and pathways that might be involved in COPD development in WT animals we examined the lung mRNA expression profile of four and six months CS-exposed versus FA-exposed mice by microarray analysis using the Illumina Mouse Ref-8 v2.0 BeadChip. CS exposure induced a strong activation of two pathways: "innate and adaptive immune cell communication" and "IL-10 signaling", among others (Table 1, Figure 7A). We selected two regulated genes involved in these pathways and confirmed by an independent experiment the significant increases in mRNA expression of TNF-α (Figure 5B) and IL1RN (Figure 7B).

Recently, it was shown that B cells are capable of polarizing macrophages to an alternatively activated phenotype via secretion of IL-10 (56). Therefore, we first investigated via qPCR whether IL-10 was upregulated in our smoke model. Though IL-10 mRNA expression levels were higher in CS-exposed μMT compared to WT mice at 1 month, IL-10 mRNA expression increased significantly in WT animals at 6 months of CS exposure (Figure 8A). Immunohistochemistry of WT lung tissue for IL-10 demonstrated strong staining in areas of inflammatory cell accumulation consisting predominantly of CD45R-positive B cells but not in CD3 positive T cells (Figure 8B).

Finally, *in vitro* stimulation of the murine B cell line A20 for 24 hours with two concentrations of CS extract (CS 1 and 4%) showed increases in IL-10 mRNA expression and secretion after stimulation with both CS extract concentrations (Figure 8C, D). In contrast,

464 increased mRNA expression of inflammatory genes such as IL-6, TNF-α and GM-CSF was
465 only observed in positive control (LPS)-treated cells (fold increase compared to control: 2.5 ±
466 0.2 for IL-6, 1.5 ± 0.1 for TNF-α, 8.5 ± 1.1 for GM-CSF).

467 To confirm the role for B cells in influencing macrophage activation, we treated the
468 macrophage cell line MH-S for 6 hours with LPS and CS extract as well as with supernatants
469 obtained from A20 cells stimulated with LPS or CS extract (1 and 4%) for 24 hours. qPCR
470 analysis of MMP12 showed a strong increase in mRNA expression when MH-S cells where
471 stimulated with supernatants from CS extract-treated A20 cells. Furthermore, to evaluate the
472 possible role of B cell-derived IL-10, we aimed at blocking IL-10 signaling in MH-S cells
473 treated with A20 supernatants by including an anti-IL-10 antibody. This led to a significant
474 reduction of MMP12 expression in MH-S cells stimulated with supernatants from CS extract-
475 treated A20 cells (Figure 8E). These data indicate that B cell-derived IL-10 is involved in
476 macrophage polarization and MMP12 upregulation after CS exposure *in vivo* as well as *in*
477 *vitro*.

478

Discussion

Our study aimed at investigating the relationship between B cell-dependent iBALT formation and the immunopathogenesis of COPD. We identified what we believe to be a major pathway that induces and maintains the severe inflammatory response causing subsequent emphysema development in COPD. The results presented here demonstrate that B cells are involved in at least two mechanisms after CS exposure: firstly, B cells are organized in iBALT and secondly, they were found to be potent regulators of macrophage accumulation and macrophage-derived MMP12 production thereby contributing to emphysema development.

There is considerable evidence that the CS-induced inflammatory response plays a major role in driving the pathophysiological changes observed in COPD (5, 12). Due to the high toxicity of both its gaseous and particle phases (9, 47), CS persistently induces a neutrophil and macrophage inflammatory response in the lower respiratory tract of both humans and animals exposed in experimental models (11, 24, 49). While the acute reaction during the first week of CS exposure is dominated by a strong neutrophilic and macrophage influx, the chronic phase starting from 1 month of CS exposure is additionally characterized by infiltration of adaptive immune cells, i.e. lymphocytes, and by progressive pathophysiological changes similar to those observed in COPD patients, such as small airway remodeling and septal tissue damage/emphysema (13, 46, 54). In our current study, we found that B cell deficient animals develop emphysematous changes in an elastase mouse model (Figure 4); however, these animals were protected against CS-induced emphysema development (Figure 3). In contrast, WT mice show functional and structural lung changes after 4 months of CS exposure and this coincides with B cell accumulation.

TLOs formed in the lung belong to inducible bronchus-associated lymphoid tissue (iBALT), which is defined as ectopic lymphoid tissue induced in response to infection or inflammation.

503 This allows local priming and clonal expansion of B and T cells, antigen retention, somatic
504 hypermutation, affinity maturation and immunoglobulin (Ig) class switching (1, 28). By
505 acquiring antigens from the airways, iBALT induces a local inflammatory response and is
506 responsible for the maintenance of memory cells in the lungs (41). Therefore, iBALT may be
507 beneficial for the host by providing protection against microbial colonization and infection of
508 the lower respiratory tract. Several studies have shown a protective role for iBALT-related
509 local immune responses in the context of influenza infection (34, 43). However, the immune
510 response mediated by iBALTs might also be of a harmful nature in COPD patients. Two
511 recent studies investigated lymphoid neogenesis in the COPD lung and confirmed the
512 important role of CXCL13 (6, 29). Litsiou *et al.* found that CXCL13 levels correlate with LF
513 density in COPD patients and that CXCL13 promotes B cell migration to ectopic sites of
514 lymphoid tissue formation in the lung (29). Bracke *et al.* performed prophylactic and
515 therapeutic treatment with an anti-CXCL13 antibody in mice exposed to CS for 6 months (6).
516 This inhibited the formation of pulmonary LFs and led to an attenuated BAL inflammation
517 and a partial protection against destruction of alveolar walls. We were also able to confirm an
518 upregulation of CXCL13 after CS exposure in WT mice. Furthermore, the prevention of
519 iBALT formation in μMT mice inhibited COPD development in our study (Figure 1 and 3).

520 This strongly points to an involvement of iBALT formation in COPD pathogenesis, but the
521 exact contribution to disease development still remains unclear. Recent studies, mostly from
522 the field of autoimmune diseases such as multiple sclerosis (22, 55) and rheumatoid arthritis
523 (51) have focused their attention on the possible B cell roles that are independent of their
524 lymphoid neogenesis and antibody secreting function. Further potent effector functions
525 include antigen presentation, T cell activation and regulation as well as secretion of a variety
526 of immunmodulatory cytokines such as IL-6 and IL-10 (15, 23). Interestingly, cytokine
527 secretion by B cells has been shown to influence and modulate differentiation and polarization

of T cells, macrophages and dendritic cells during the development of the immune response thereby regulating immune reactions (23). Moreover, macrophage effector functions can be directly regulated by B cell-mediated cytokine secretion, which was shown to be important for the outcome of various models of infection, inflammation and cancer. Kelly-Scumpia *et al.* demonstrated that B cell-dependent cytokine responses are required for and enhance early innate immune responses during bacterial sepsis (26). During viral infection with VSV, B cells are indispensable for providing lymphotoxin and thereby maintaining an antiviral macrophage phenotype that protects against fatal CNS invasion (32).

An important role has been attributed to B cell-derived IL-10 in various disease models. Increased production of anti-inflammatory IL-10 by B cells in multiple sclerosis, lupus and rheumatoid arthritis patients is capable of downregulating T cell responses (19, 22). IL-10-producing B cells were also shown to regulate macrophage function by decreasing their phagocytic activity and cytokine and NO production (25, 39). The modulated phagocytic activity of macrophages was described as facilitating fungal infection in mice (38). Interestingly, B1 cells, a B cell subset predominantly located in peritoneal and pleural cavities, were described as the main source of B cell-derived IL-10 (31), and IL-10 secreted by these cells plays a role in polarizing macrophages to an M2-like phenotype that promotes tumor growth in a melanoma model (56), and modulates wound-healing processes in mice (35).

Macrophages are involved in the severe chronic lung inflammation observed in COPD. In response to CS, macrophages release cytokines and proteolytic enzymes and generate oxidants, thereby causing tissue damage and perpetuating inflammation and immune reactions (49). Because MMP12 knockout mice are protected against CS-induced macrophage recruitment and emphysema development, these cells and their derived factors seem to be

552 required for disease onset and progression (18). Here, we showed strong differences in lung
553 tissue inflammation between WT and μMT mice, with significant increases in tissue
554 macrophages and upregulated MMP12 expression in CS-exposed WT mice (Figure 6).
555 Moreover, we identified a role for B cell-derived IL-10 in enhancing macrophage activation
556 and MMP12 upregulation (Figure 8). To our knowledge, our data are the first to provide a
557 link between macrophages and B cells involved in COPD pathogenesis.

558 Interestingly, CXCL13 neutralization was also shown to directly affect macrophages (6).
559 Bracke *et al.* found reduced expression of MMP12 in macrophages of CS-exposed, anti-
560 CXCL13-treated mice, which confirms our findings of B cell-mediated MMP12 induction in
561 macrophages. However, because CXCL13 treatment did not significantly alter lung
562 inflammation, alveolar enlargement and airway remodeling in their study, the authors
563 concluded that the innate immune system might be sufficient to induce emphysema after CS
564 exposure, as shown by D'hulst *et al.* using severe combined immunodeficiency (scid) mice,
565 which lack B and T lymphocytes (12). These animals developed emphysema after CS
566 exposure. But since scid mice are from a BALB/c background, results are difficult to compare
567 to our study. Nevertheless, CS exposure of scid and anti-CXCL13-treated mice also revealed
568 a marked increase in lung macrophages and MMP12 expression. Based on these findings, we
569 suggest that further investigation and targeting of B cells or especially IL-10-releasing B cells
570 in the formation of iBALT and subsequent emphysema development in a CS-induced COPD
571 mouse model may shed further light on mechanisms that could induce reparative and
572 regenerative processes in the COPD lung.

573 In conclusion, we have shown that CS exposure leads to B cell-dependent iBALT formation,
574 which contributes to the pathogenesis of COPD via IL-10-induced macrophage activation and
575 MMP12 upregulation. Unraveling the mechanisms that are involved in and link innate and

adaptive immune cell responses to CS in COPD is of great clinical relevance. The significant role for B cells and iBALT formation in CS-induced emphysema development provides a new innovative mechanism, which could be explored as a target for therapeutic intervention in COPD patients. Targeting iBALT formation in early stages after CS exposure in order to inhibit subsequent macrophage upregulation could be a promising option to prevent COPD progression.

582 **Acknowledgement**

583 The authors acknowledge the help of Bernd Lentner, Gunter Eder, Christine Hollauer and
584 Anke Bettenbrock.

585

586 **Grants**

587 This work was supported by a European Respiratory Society Fellowship awarded to Gerrit
588 John-Schuster (LTRF MC1520-2010).

589

590 **Disclosures**

591 The authors declare that they have no conflict of interest.

592

593 **Author contribution**

594 GJS, KH, MI, JB, OE & AÖY designed experiments; GJS, KH, MI & TMC conducted
595 experiments; GJS, KH & AÖY wrote the manuscript; all authors contributed to scientific
596 discussions and read the manuscript.

597

598

599

References

1. **Aloisi F and Pujol-Borrell R.** Lymphoid neogenesis in chronic inflammatory diseases. *Nat Rev Immunol* 6: 205-217, 2006.
2. **Barnes PJ, Shapiro SD, and Pauwels RA.** Chronic obstructive pulmonary disease: molecular and cellular mechanisms. *Eur Respir J* 22: 672-688, 2003.
3. **Biswas SK and Mantovani A.** Macrophage plasticity and interaction with lymphocyte subsets: cancer as a paradigm. *Nat Immunol* 11: 889-896, 2010.
4. **Bosken CH, Hards J, Gatter K, and Hogg JC.** Characterization of the inflammatory reaction in the peripheral airways of cigarette smokers using immunocytochemistry. *The American review of respiratory disease* 145: 911-917, 1992.
5. **Botelho FM, Gaschler GJ, Kianpour S, Zavitz CC, Trimble NJ, Nikota JK, Bauer CM, and Stampfli MR.** Innate immune processes are sufficient for driving cigarette smoke-induced inflammation in mice. *Am J Respir Cell Mol Biol* 42: 394-403, 2010.
6. **Bracke KR, Verhamme FM, Seys LJ, Bantsimba-Malanda C, Cunoosamy DM, Herbst R, Hammad H, Lambrecht BN, Joos GF, and Brusselle GG.** Role of CXCL13 in cigarette smoke-induced lymphoid follicle formation and chronic obstructive pulmonary disease. *Am J Respir Crit Care Med* 188: 343-355, 2013.
7. **Brusselle GG.** Matrix metalloproteinase 12, asthma, and COPD. *N Engl J Med* 361: 2664-2665, 2009.
8. **Brusselle GG, Demoor T, Bracke KR, Brandsma CA, and Timens W.** Lymphoid follicles in (very) severe COPD: beneficial or harmful? *Eur Respir J* 34: 219-230, 2009.
9. **Cantin AM.** Cellular response to cigarette smoke and oxidants: adapting to survive. *Proc Am Thorac Soc* 7: 368-375, 2010.
10. **Carragher DM, Rangel-Moreno J, and Randall TD.** Ectopic lymphoid tissues and local immunity. *Seminars in immunology* 20: 26-42, 2008.
11. **Churg A, Cosio M, and Wright JL.** Mechanisms of cigarette smoke-induced COPD: insights from animal models. *Am J Physiol Lung Cell Mol Physiol* 294: L612-631, 2008.
12. **D'Hulst A I, Maes T, Bracke KR, Demedts IK, Tournoy KG, Joos GF, and Brusselle GG.** Cigarette smoke-induced pulmonary emphysema in scid-mice. Is the acquired immune system required? *Respir Res* 6: 147, 2005.
13. **D'Hulst A I, Vermaelen KY, Brusselle GG, Joos GF, and Pauwels RA.** Time course of cigarette smoke-induced pulmonary inflammation in mice. *Eur Respir J* 26: 204-213, 2005.
14. **Dieu-Nosjean MC, Antoine M, Danel C, Heudes D, Wislez M, Poulot V, Rabbe N, Laurans L, Tartour E, de Chaisemartin L, Lebecque S, Fridman WH, and Cadranel J.** Long-term survival for patients with non-small-cell lung cancer with intratumoral lymphoid structures. *Journal of clinical oncology : official journal of the American Society of Clinical Oncology* 26: 4410-4417, 2008.
15. **DiLillo DJ, Horikawa M, and Tedder TF.** B-lymphocyte effector functions in health and disease. *Immunologic research* 49: 281-292, 2011.
16. **Gosman MM, Willemse BW, Jansen DF, Lapperre TS, van Schadewijk A, Hiemstra PS, Postma DS, Timens W, Kerstjens HA, Groningen, and Leiden Universities Corticosteroids in Obstructive Lung Disease Study G.** Increased number of B-cells in bronchial biopsies in COPD. *Eur Respir J* 27: 60-64, 2006.
17. **Halle S, Dujardin HC, Bakocevic N, Fleige H, Danzer H, Willenzon S, Suezer Y, Hammerling G, Garbi N, Sutter G, Worbs T, and Forster R.** Induced bronchus-associated lymphoid tissue serves as a general priming site for T cells and is maintained by dendritic cells. *The Journal of experimental medicine* 206: 2593-2601, 2009.
18. **Hautamaki RD, Kobayashi DK, Senior RM, and Shapiro SD.** Requirement for macrophage elastase for cigarette smoke-induced emphysema in mice. *Science* 277: 2002-2004, 1997.
19. **Heo YJ, Joo YB, Oh HJ, Park MK, Heo YM, Cho ML, Kwok SK, Ju JH, Park KS, Cho SG, Park SH, Kim HY, and Min JK.** IL-10 suppresses Th17 cells and promotes regulatory T cells in the CD4+ T cell population of rheumatoid arthritis patients. *Immunology letters* 127: 150-156, 2010.

20. **Hogg JC.** Pathophysiology of airflow limitation in chronic obstructive pulmonary disease. *Lancet* 364: 709-721, 2004.
21. **Hogg JC, Chu F, Utokaparch S, Woods R, Elliott WM, Buzatu L, Cherniack RM, Rogers RM, Sciurba FC, Coxson HO, and Pare PD.** The nature of small-airway obstruction in chronic obstructive pulmonary disease. *N Engl J Med* 350: 2645-2653, 2004.
22. **Ireland S and Monson N.** Potential impact of B cells on T cell function in multiple sclerosis. *Multiple sclerosis international* 2011: 423971, 2011.
23. **Ireland SJ, Blazek M, Harp CT, Greenberg B, Frohman EM, Davis LS, and Monson NL.** Antibody-independent B cell effector functions in relapsing remitting multiple sclerosis: clues to increased inflammatory and reduced regulatory B cell capacity. *Autoimmunity* 45: 400-414, 2012.
24. **John G, Kohse K, Orasche J, Reda A, Schnelle-Kreis J, Zimmermann R, Schmid O, Eickelberg O, and Yildirim AO.** The composition of cigarette smoke determines inflammatory cell recruitment to the lung in COPD mouse models. *Clinical science* 126: 207-221, 2014.
25. **Kalampokis I, Yoshizaki A, and Tedder TF.** IL-10-producing regulatory B cells (B10 cells) in autoimmune disease. *Arthritis research & therapy* 15 Suppl 1: S1, 2013.
26. **Kelly-Scumpia KM, Scumpia PO, Weinstein JS, Delano MJ, Cuenca AG, Nacionales DC, Wynn JL, Lee PY, Kumagai Y, Efron PA, Akira S, Wasserfall C, Atkinson MA, and Moldawer LL.** B cells enhance early innate immune responses during bacterial sepsis. *The Journal of experimental medicine* 208: 1673-1682, 2011.
27. **Kitamura D, Roes J, Kuhn R, and Rajewsky K.** A B cell-deficient mouse by targeted disruption of the membrane exon of the immunoglobulin mu chain gene. *Nature* 350: 423-426, 1991.
28. **Kroese FG, Timens W, and Nieuwenhuis P.** Germinal center reaction and B lymphocytes: morphology and function. *Current topics in pathology Ergebnisse der Pathologie* 84 (Pt 1): 103-148, 1990.
29. **Litsiou E, Semitekolou M, Galani IE, Morianos I, Tsoutsa A, Kara P, Rontogianni D, Bellenis I, Konstantinou M, Potaris K, Andreakos E, Sideras P, Zakynthinos S, and Tsoumakidou M.** CXCL13 production in B cells via Toll-like receptor/lymphotoxin receptor signaling is involved in lymphoid neogenesis in chronic obstructive pulmonary disease. *Am J Respir Crit Care Med* 187: 1194-1202, 2013.
30. **Lucey EC, Keane J, Kuang PP, Snider GL, and Goldstein RH.** Severity of elastase-induced emphysema is decreased in tumor necrosis factor-alpha and interleukin-1beta receptor-deficient mice. *Laboratory investigation; a journal of technical methods and pathology* 82: 79-85, 2002.
31. **Minoprio P, el Cheikh MC, Murphy E, Hontebeyrie-Joskowicz M, Coffman R, Coutinho A, and O'Garra A.** Xid-associated resistance to experimental Chagas' disease is IFN-gamma dependent. *J Immunol* 151: 4200-4208, 1993.
32. **Moseman EA, Iannacone M, Bosurgi L, Tonti E, Chevrier N, Tumanov A, Fu YX, Hacohen N, and von Andrian UH.** B cell maintenance of subcapsular sinus macrophages protects against a fatal viral infection independent of adaptive immunity. *Immunity* 36: 415-426, 2012.
33. **Motallebzadeh R, Rehakova S, Conlon TM, Win TS, Callaghan CJ, Goddard M, Bolton EM, Ruddle NH, Bradley JA, and Pettigrew GJ.** Blocking lymphotoxin signaling abrogates the development of ectopic lymphoid tissue within cardiac allografts and inhibits effector antibody responses. *FASEB journal : official publication of the Federation of American Societies for Experimental Biology* 26: 51-62, 2012.
34. **Moyron-Quiroz JE, Rangel-Moreno J, Kusser K, Hartson L, Sprague F, Goodrich S, Woodland DL, Lund FE, and Randall TD.** Role of inducible bronchus associated lymphoid tissue (iBALT) in respiratory immunity. *Nat Med* 10: 927-934, 2004.
35. **Oliveira HC, Popi AF, Bachi AL, Nonogaki S, Lopes JD, and Mariano M.** B-1 cells modulate the kinetics of wound-healing process in mice. *Immunobiology* 215: 215-222, 2010.
36. **Pauwels RA, Buist AS, Calverley PM, Jenkins CR, and Hurd SS.** Global strategy for the diagnosis, management, and prevention of chronic obstructive pulmonary disease. NHLBI/WHO Global Initiative for Chronic Obstructive Lung Disease (GOLD) Workshop summary. *Am J Respir Crit Care Med* 163: 1256-1276, 2001.

37. **Perros F, Dorfmuller P, Montani D, Hammad H, Waelput W, Girerd B, Raymond N, Mercier O, Mussot S, Cohen-Kaminsky S, Humbert M, and Lambrecht BN.** Pulmonary lymphoid neogenesis in idiopathic pulmonary arterial hypertension. *Am J Respir Crit Care Med* 185: 311-321, 2012.
38. **Popi AF, Godoy LC, Xander P, Lopes JD, and Mariano M.** B-1 cells facilitate Paracoccidioides brasiliensis infection in mice via IL-10 secretion. *Microbes and infection / Institut Pasteur* 10: 817-824, 2008.
39. **Popi AF, Lopes JD, and Mariano M.** Interleukin-10 secreted by B-1 cells modulates the phagocytic activity of murine macrophages in vitro. *Immunology* 113: 348-354, 2004.
40. **Rainer J, Sanchez-Cabo F, Stocker G, Sturn A, and Trajanoski Z.** CARMAweb: comprehensive R- and bioconductor-based web service for microarray data analysis. *Nucleic acids research* 34: W498-503, 2006.
41. **Randall TD.** Bronchus-associated lymphoid tissue (BALT) structure and function. *Advances in immunology* 107: 187-241, 2010.
42. **Rangel-Moreno J, Hartson L, Navarro C, Gaxiola M, Selman M, and Randall TD.** Inducible bronchus-associated lymphoid tissue (iBALT) in patients with pulmonary complications of rheumatoid arthritis. *J Clin Invest* 116: 3183-3194, 2006.
43. **Rangel-Moreno J, Moyron-Quiroz JE, Hartson L, Kusser K, and Randall TD.** Pulmonary expression of CXC chemokine ligand 13, CC chemokine ligand 19, and CC chemokine ligand 21 is essential for local immunity to influenza. *Proceedings of the National Academy of Sciences of the United States of America* 104: 10577-10582, 2007.
44. **Saetta M, Di Stefano A, Turato G, Facchini FM, Corbino L, Mapp CE, Maestrelli P, Ciaccia A, and Fabbri LM.** CD8+ T-lymphocytes in peripheral airways of smokers with chronic obstructive pulmonary disease. *Am J Respir Crit Care Med* 157: 822-826, 1998.
45. **Saetta M, Turato G, Facchini FM, Corbino L, Lucchini RE, Casoni G, Maestrelli P, Mapp CE, Ciaccia A, and Fabbri LM.** Inflammatory cells in the bronchial glands of smokers with chronic bronchitis. *Am J Respir Crit Care Med* 156: 1633-1639, 1997.
46. **Stevenson CS, Docx C, Webster R, Battram C, Hynx D, Giddings J, Cooper PR, Chakravarty P, Rahman I, Marwick JA, Kirkham PA, Charman C, Richardson DL, Nirmala NR, Whittaker P, and Butler K.** Comprehensive gene expression profiling of rat lung reveals distinct acute and chronic responses to cigarette smoke inhalation. *Am J Physiol Lung Cell Mol Physiol* 293: L1183-1193, 2007.
47. **Takahashi Y, Horiyama S, Honda C, Suwa K, Nakamura K, Kunitomo M, Shimma S, Toyoda M, Sato H, Shizuma M, and Takayama M.** A chemical approach to searching for bioactive ingredients in cigarette smoke. *Chemical & pharmaceutical bulletin* 61: 85-89, 2013.
48. **Team RDC.** R: A language and environment for statistical computing: ISBN 3-900051-07-0. R Foundation for Statistical Computing. Vienna, Austria, 2013. url: http://www. R-project. org, 2005.
49. **Tetley TD.** Inflammatory cells and chronic obstructive pulmonary disease. *Current drug targets Inflammation and allergy* 4: 607-618, 2005.
50. **Thun MJ, Carter BD, Feskanich D, Freedman ND, Prentice R, Lopez AD, Hartge P, and Gapstur SM.** 50-Year Trends in Smoking-Related Mortality in the United States. *New England Journal of Medicine* 368: 351-364, 2013.
51. **van de Veerdonk FL, Lauwerys B, Marijnissen RJ, Timmermans K, Di Padova F, Koenders MI, Gutierrez-Roelens I, Durez P, Netea MG, van der Meer JW, van den Berg WB, and Joosten LA.** The anti-CD20 antibody rituximab reduces the Th17 cell response. *Arthritis and rheumatism* 63: 1507-1516, 2011.
52. **van der Strate BW, Postma DS, Brandsma CA, Melgert BN, Luinge MA, Geerlings M, Hylkema MN, van den Berg A, Timens W, and Kerstjens HA.** Cigarette smoke-induced emphysema: A role for the B cell? *Am J Respir Crit Care Med* 173: 751-758, 2006.
53. **Vestbo J, Hurd SS, Agusti AG, Jones PW, Vogelmeier C, Anzueto A, Barnes PJ, Fabbri LM, Martinez FJ, Nishimura M, Stockley RA, Sin DD, and Rodriguez-Roisin R.** Global strategy for the diagnosis, management, and prevention of chronic obstructive pulmonary disease: GOLD executive summary. *Am J Respir Crit Care Med* 187: 347-365, 2013.

54. **Wan WY, Morris A, Kinnear G, Pearce W, Mok J, Wyss D, and Stevenson CS.** Pharmacological characterisation of anti-inflammatory compounds in acute and chronic mouse models of cigarette smoke-induced inflammation. *Respir Res* 11: 126, 2010.
55. **Weber MS, Prod'homme T, Patarroyo JC, Molnarfi N, Karnezis T, Lehmann-Horn K, Danilenko DM, Eastham-Anderson J, Slavin AJ, Linington C, Bernard CC, Martin F, and Zamvil SS.** B-cell activation influences T-cell polarization and outcome of anti-CD20 B-cell depletion in central nervous system autoimmunity. *Annals of neurology* 68: 369-383, 2010.
56. **Wong SC, Puaux AL, Chittezhath M, Shalova I, Kajiji TS, Wang X, Abastado JP, Lam KP, and Biswas SK.** Macrophage polarization to a unique phenotype driven by B cells. *European journal of immunology* 40: 2296-2307, 2010.
57. **Yadava K and Marsland BJ.** Lymphoid follicles in chronic lung diseases. *Thorax* 68: 597-598, 2013.
58. **Ye J, Coulouris G, Zaretskaya I, Cutcutache I, Rozen S, and Madden TL.** Primer-BLAST: a tool to design target-specific primers for polymerase chain reaction. *BMC bioinformatics* 13: 134, 2012.
59. **Yildirim AO, Muyal V, John G, Muller B, Seifart C, Kasper M, and Fehrenbach H.** Palifermin induces alveolar maintenance programs in emphysematous mice. *Am J Respir Crit Care Med* 181: 705-717, 2010.

Figure captions

Figure 1. Chronic CS exposure leads to inflammatory cell recruitment and inducible bronchus-associated lymphoid tissue (iBALT) formation in lungs of WT mice. Data were combined from 2 independent experiments (8 mice per group and per time points) and are given as mean values ± SD; one-way ANOVA following Bonferroni post test with **p* <0.05, ***p* <0.01, ****p* <0.001.

A. Representative micrographs of HE-stained lung tissue sections from FA and CS-exposed WT mice versus FA and CS-exposed μMT mice at indicated time points; scale bar 200 μm.

B. Volume of iBALT per basal membrane was determined via quantitative morphological assessment.

C. mRNA expression of CXCL13 in lung tissue was measured by qPCR and data are presented as relative expression to house-keeping control HPRT-1.

D & E. Immunhistochemistry for CD45R and CD3 in lung tissue from FA and CS-exposed WT mice (D) versus FA and CS-exposed μMT mice (E) at indicated time points.

Figure 2. Staining for B cells and CD4 positive Th subsets in lung tissue after chronic CS exposure reveals increases in B cells and Th17 cells in WT mice. For flow cytometric analysis single-cell suspensions were prepared from lung tissue. Surface marker stainings were directly performed with single-cell suspensions. For intracellular cytokine stainings, mononuclear cells were isolated from total lung cells by density gradient purification, stimulated overnight and restimulated for 4h prior to fixation, permeabilization and intracellular staining (see representative FACS plots for each staining performed). Data were

802 combined from 2 independent experiments (4-6 mice per group and per time points) and are
803 given as mean values ± SD; one-way ANOVA following Bonferroni post test with *p <0.05,
804 **p <0.01, ***p <0.001.
805 **A.** Mature B cells defined by expression of CD20 in FA and CS-exposed WT mice.
806 **B.** Gating strategy for lung CD4+ T cells expressing either IFN-γ (Th1), IL-4 (Th2) or IL-17
807 (Th17) or different combinations thereof.
808 **C., D. & E:** Th1 cells (C), Th2 cells (D) and Th17 cells (E)in FA and CS-exposed WT mice
809 versus FA and CS-exposed μMT mice.
810
811
812 **Figure 3. B cell deficiency protects against airspace enlargement and lung dysfunction**
813 **after chronic CS exposure.** Data were combined from 2 independent experiments (8 mice
814 per group and per time points) and are given as mean values ± SD; one-way ANOVA
815 following Bonferroni post test with *p <0.05, **p <0.01, ***p <0.001.
816 **A.** Representative micrographs of FA and CS-exposed WT mice versus FA and CS-exposed
817 μMT mice at indicated time points; scale bar 200 μm.
818 **B.** Quantitative measurement of emphysema was determined by design-based stereology of
819 HE-stained lung tissue sections using an Olympus BX51 light microscope equipped with
820 the computer-assisted stereological toolbox newCAST.
821 **C.** Lung function measurements for dynamic compliance were performed in chronic CS-
822 exposed WT and μMT mice after 1, 4 and 6 months.
823 **D.** Body weight changes are given in [%] compared to the respective FA controls.
824
825 **Figure 4. Elastase treatment results in severe pulmonary emphysema after 28 days in**
826 **both WT and μMT mice.** Data were combined from 2 independent experiments (8 mice per

group) and are given as mean values ± SD; one-way ANOVA following Bonferroni post test with *p <0.05, **p <0.01, ***p <0.001.

A. C57BL/6 mice were treated with porcine pancreatic elastase to induce emphysema. Representative micrographs of hematoxylin and eosin (HE)-stained lung tissue slides reveal emphysema development after 28 d; scale bar 200 µm.

B. Quantitative morphological assessment demonstrated airspace enlargement as indicated by significant increases in mean linear intercept (MLI) for both groups.

C. Lung function measurements revealed significantly increased lung compliance.

Figure 5. BAL and lung tissue inflammation is similar in WT and µMT mice after chronic CS exposure. Data were combined from 2 independent experiments (8 mice per group) and are given as mean values ± SD; one-way ANOVA following Bonferroni post test with *p <0.05, **p <0.01, ***p <0.001.

A. The lungs of WT and µMT mice were lavaged with 4 x 0.5 ml aliquots of sterile PBS. BAL cytokine secretion of TNF-α, KC and MCP1 was determined using a magnetic bead-based multiplex assay. For this assay, BAL fluid was concentrated (10x) by ultrafiltration in centrifugal filter devices.

B. Lung mRNA expression levels of target genes TNF-α, KC and MCP1 in comparison to housekeeping control HPRT-1 were determined via qPCR using cDNA synthesized from lung tissue homogenate.

Figure 6. Macrophage markers are increased in the lungs of CS-exposed WT mice. Data were combined from 2 independent experiments (8 mice per group and per time points) and are given as mean values ± SD; one-way ANOVA following Bonferroni post test with *p <0.05, **p <0.01, ***p <0.001.

A. Representative micrographs of immunohistochemical stainings for MMP12 in lung sections from FA controls and CS-exposed WT and μMT mice at indicated time points; scale bar 200 μm.

B. Quantitative analysis ofMMP12-expressing macrophage numbers in lung tissue revealed significantly higher values for CS-exposed WT compared to μMT mice.

C., D. & E. Whole lung mRNA expression levels of macrophage markers F4/80 (C) and MMP12 (D) as well as the ratio of MMP12/TIMP1 (E) were investigated in comparison to housekeeping control HPRT-1 by qPCR. Relative transcript expression of target genes is given as $2^{-\Delta CT}$ ($\Delta Ct = Ct_{target} - Ct_{reference}$), relative changes compared to control are $2^{-\Delta\Delta Ct}$ values ($\Delta\Delta Ct = \Delta Ct_{treated} - \Delta Ct_{control}$). Mean values ± SD; one-way ANOVA following Bonferroni post test with $*p < 0.05$, $**p < 0.01$, $***p < 0.001$.

F. Representative western blot and densitometric analysis for MMP12 in lung tissue homogenate from WT and μMT mice after 6 months of CS exposure. β-actin was used as loading control.

G. Whole lung mRNA expression levels of M1 macrophage markers iNOS and IL-6 and M2 markers FIZZ1 and Mrc1 were investigated in comparison to housekeeping control HPRT-1 by qPCR.

Figure 7. Microarray analysis of four and six months CS-exposed versus FA-exposed mice.

A. Heat map depicting regulated genes from the two strongly activated pathways ’innate and adaptive immune cell communication’ and ‘IL-10 signaling’.

B. Whole lung mRNA expression levels of IL1RN in WT and μMT mice after 4 and 6 months of CS exposure were investigated in comparison to housekeeping control HPRT-1 by qPCR.

Figure 8. B cell-derived IL-10 secretion upregulates MMP12 expression. *In vivo* data from 2 independent experiments (8 mice per group and per time point) and *in vitro* data from 3 independent experiments were combined and are given as mean values ± SD; one-way ANOVA following Bonferroni post test with $*p < 0.05$, $**p < 0.01$, $***p < 0.001$. A20-sup: supernatant from A20 cells; CS= cigarette smoke extract.

A. IL-10 mRNA expression levels in lung tissue homogenates were investigated in comparison to housekeeping control HPRT-1 by qPCR.

B. Representative micrographs of immunohistochemical stainings for IL-10 and CD3 and for IL10 and CD45R in lung serial sections from CS-exposed WT mice after 6 months of CS exposure; scale bar 200 μm.

C. At 24h post cigarette smoke extract (CS) stimulation mRNA expression levels of IL-10 were significantly elevated in the B cell lymphoma line A20 as measured in comparison to housekeeping control HPRT-1 by qPCR.

D. IL-10 cytokine secretion in cigarette smoke extract (CS) stimulated B cell lymphoma line A20 were investigated by ELISA of cell culture supernatants.

E. MMP12 mRNA expression levels in the macrophage cell line MH-S with and without anti-IL10 antibody treatment were investigated in comparison to housekeeping control HPRT-1 by qPCR.

Figure 1

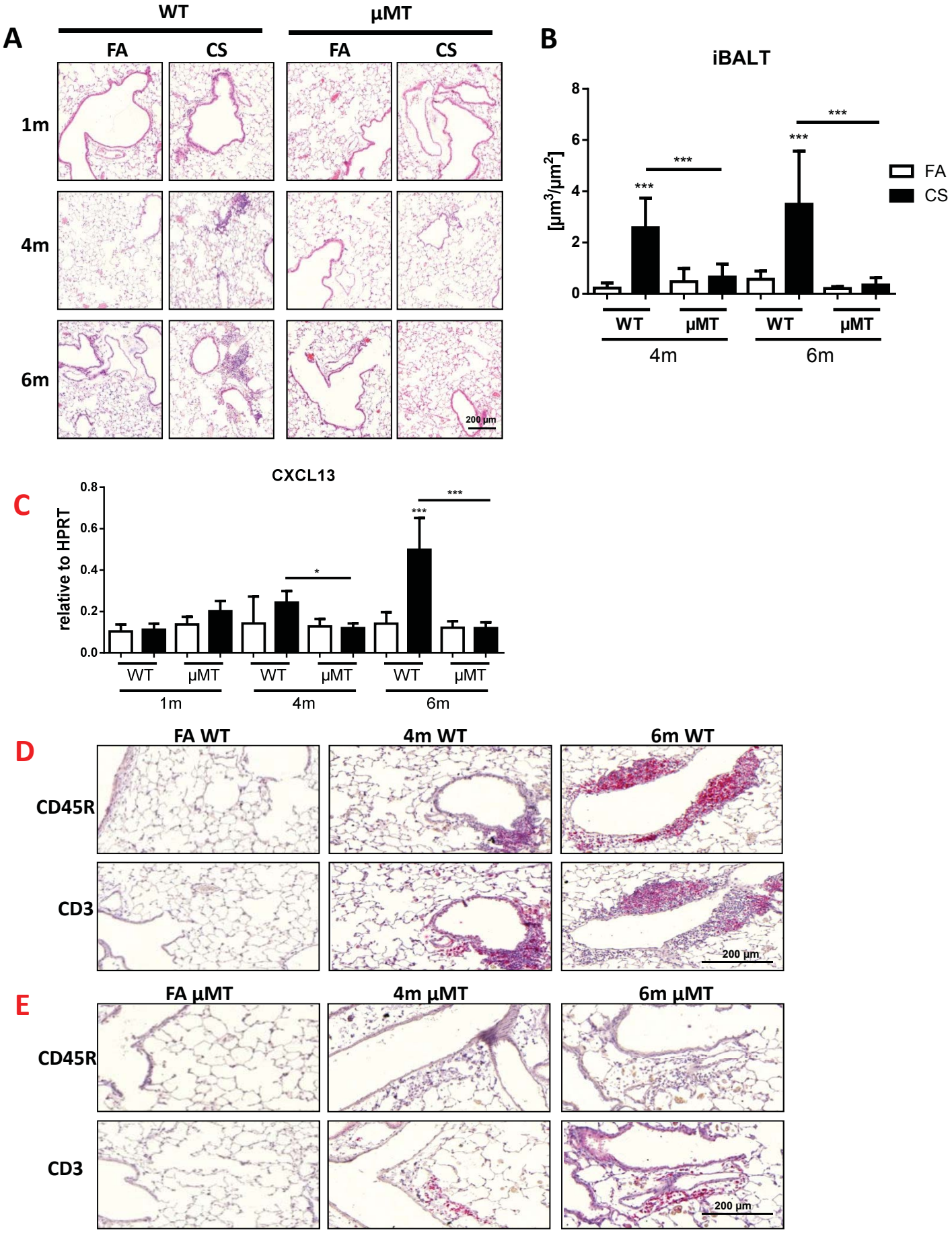
A
WT
µMT
FA
CS
FA
CS
1m
4m
6m
200 µm
B
iBALT
[µm³/µm²]
FA
CS
WT
µMT
WT
µMT
4m
6m
C
CXCL13
relative to HPRT
WT
µMT
WT
µMT
WT
µMT
1m
4m
6m
D
FA WT
4m WT
6m WT
CD45R
CD3
200 µm
E
FA µMT
4m µMT
6m µMT
CD45R
CD3
200 µm

Figure 2

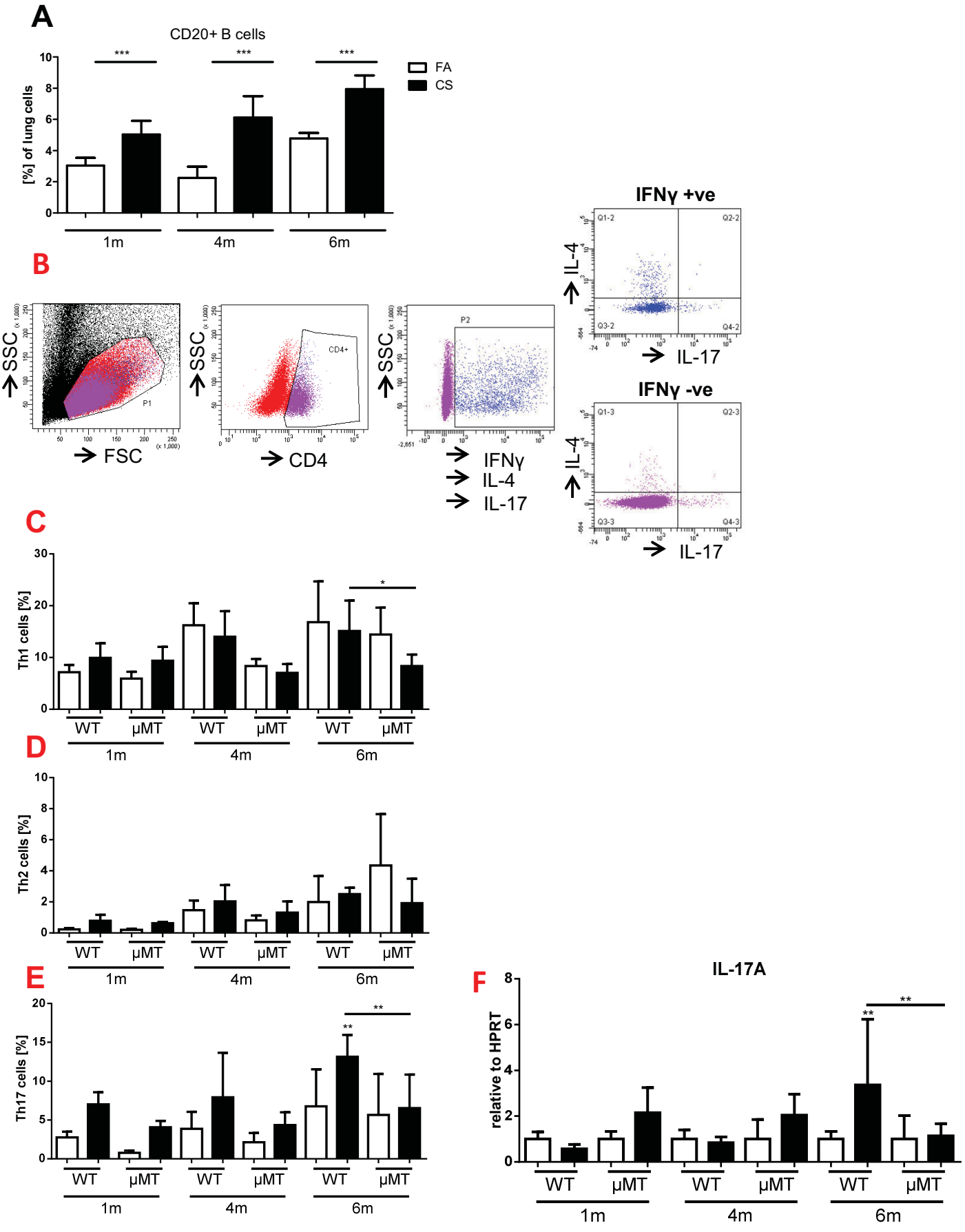
A
CD20+ B cells
[%] of lung cells
FA
CS
1m
4m
6m
B
SSC
FSC
P1
CD4+
CD4
P2
IFNγ
IL-4
IL-17
IFNγ +ve
IFNγ -ve
Q1-2
Q2-2
Q3-2
Q4-2
Q1-3
Q2-3
Q3-3
Q4-3
C
Th1 cells [%]
D
Th2 cells [%]
E
Th17 cells [%]
WT
µMT
F
IL-17A
relative to HPRT

Figure 3

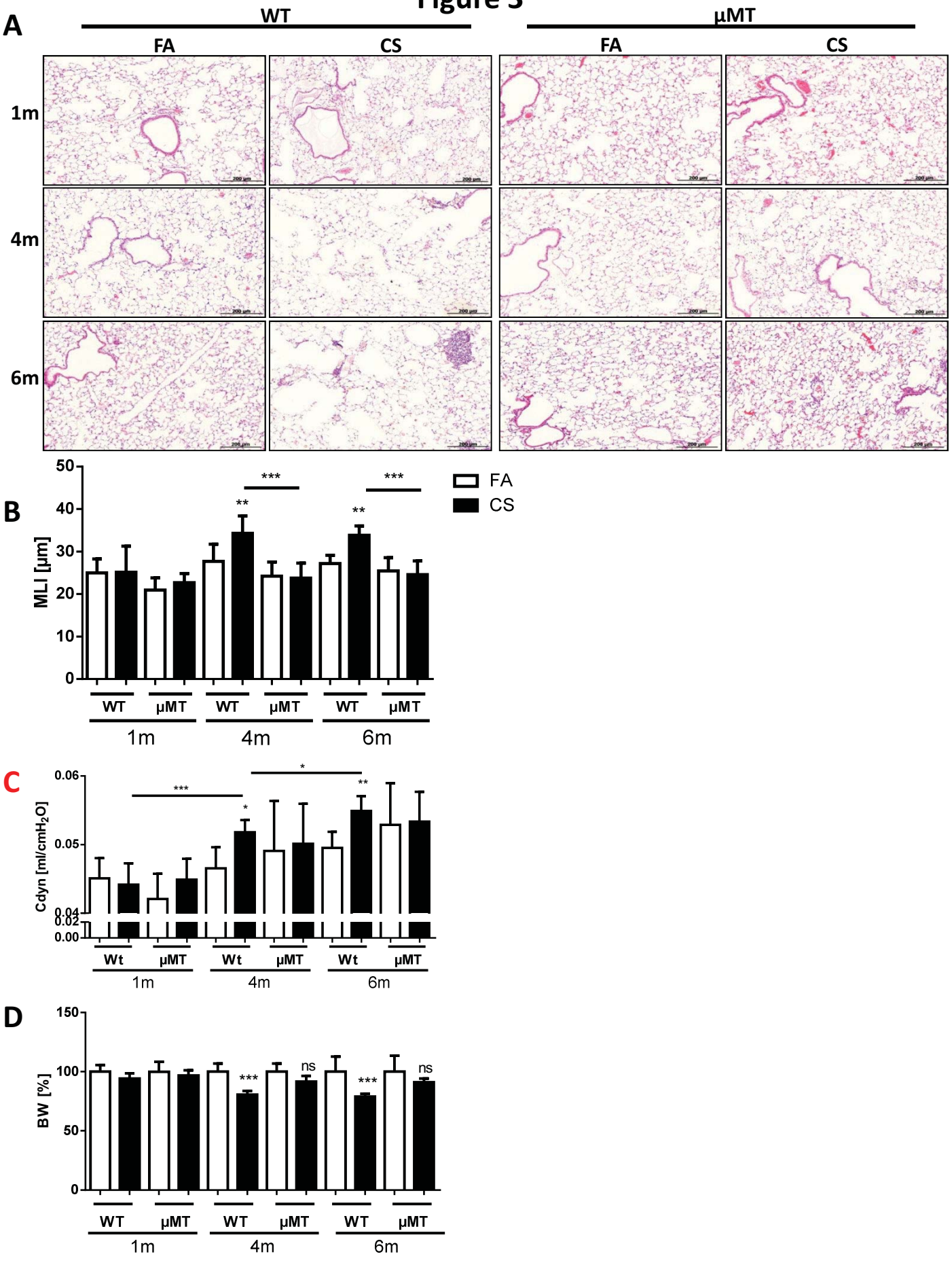
A
WT
µMT
FA
CS
FA
CS
1m
4m
6m
B
MLI [µm]
FA
CS
***
**
***
**
WT
µMT
WT
µMT
WT
µMT
1m
4m
6m
C
Cdyn [ml/cmH2O]
***
*
*
**
Wt
µMT
Wt
µMT
Wt
µMT
1m
4m
6m
D
BW [%]
***
ns
***
ns
WT
µMT
WT
µMT
WT
µMT
1m
4m
6m

Figure 4

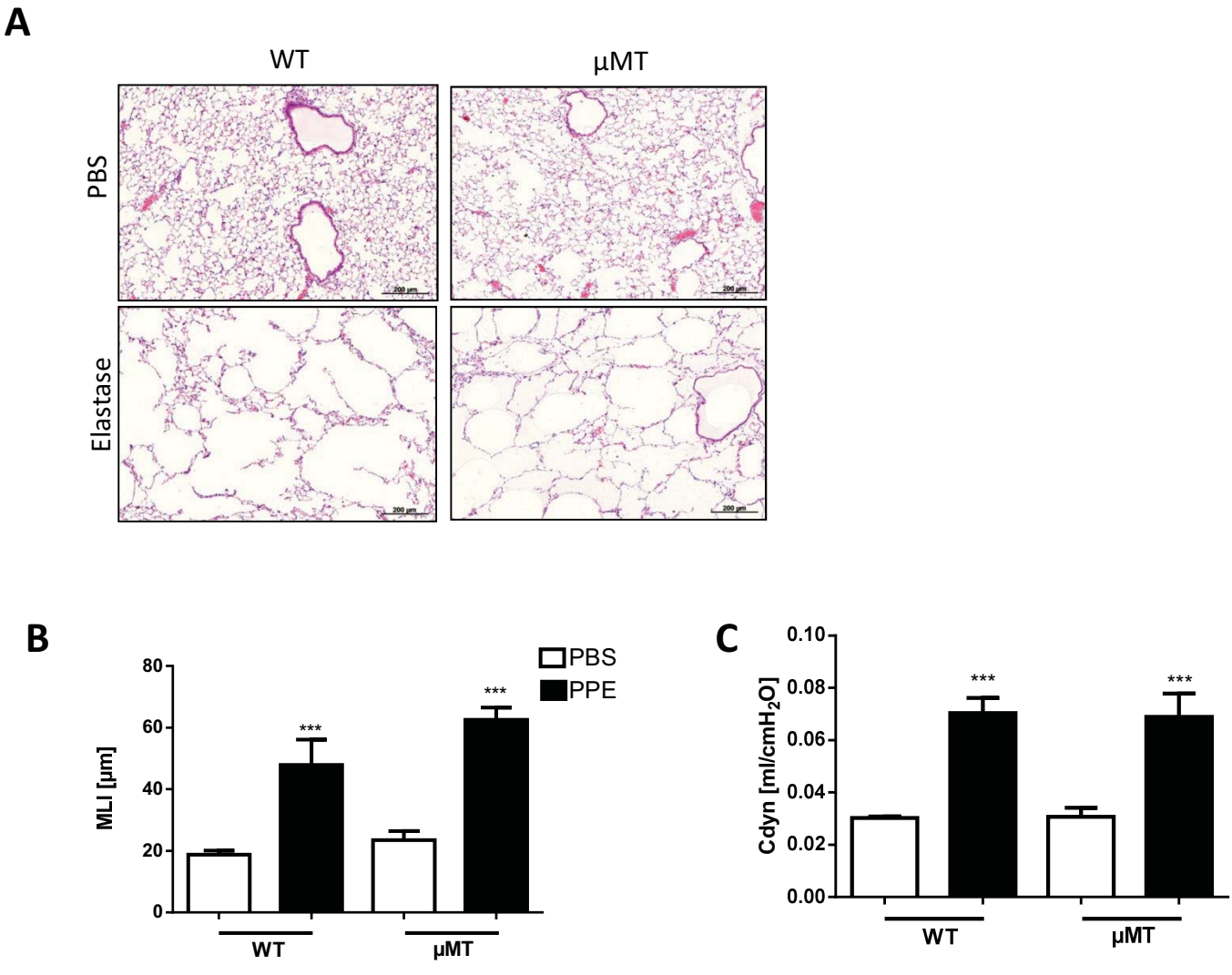
A
WT
µMT
PBS
Elastase
B
PBS
PPE
MLI [µm]
80
60
40
20
0
***
***
WT
µMT
C
Cdyn [ml/cmH2O]
0.10
0.08
0.06
0.04
0.02
0.00
***
***
WT
µMT

Figure 5- new

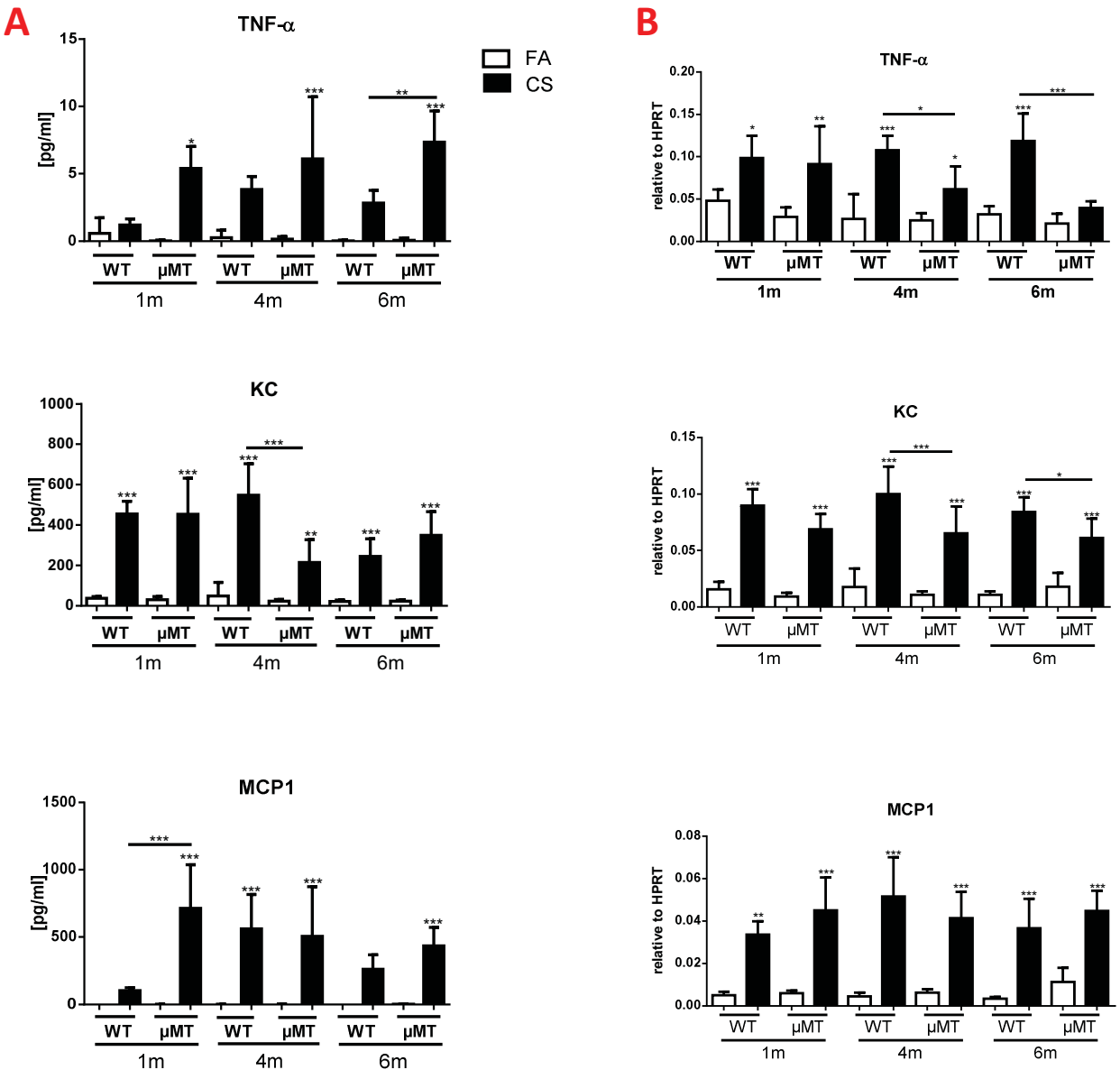
A
TNF-α
FA
CS
[pg/ml]
WT
µMT
1m
4m
6m
KC
MCP1
B
TNF-α
relative to HPRT
KC
MCP1

Figure 6

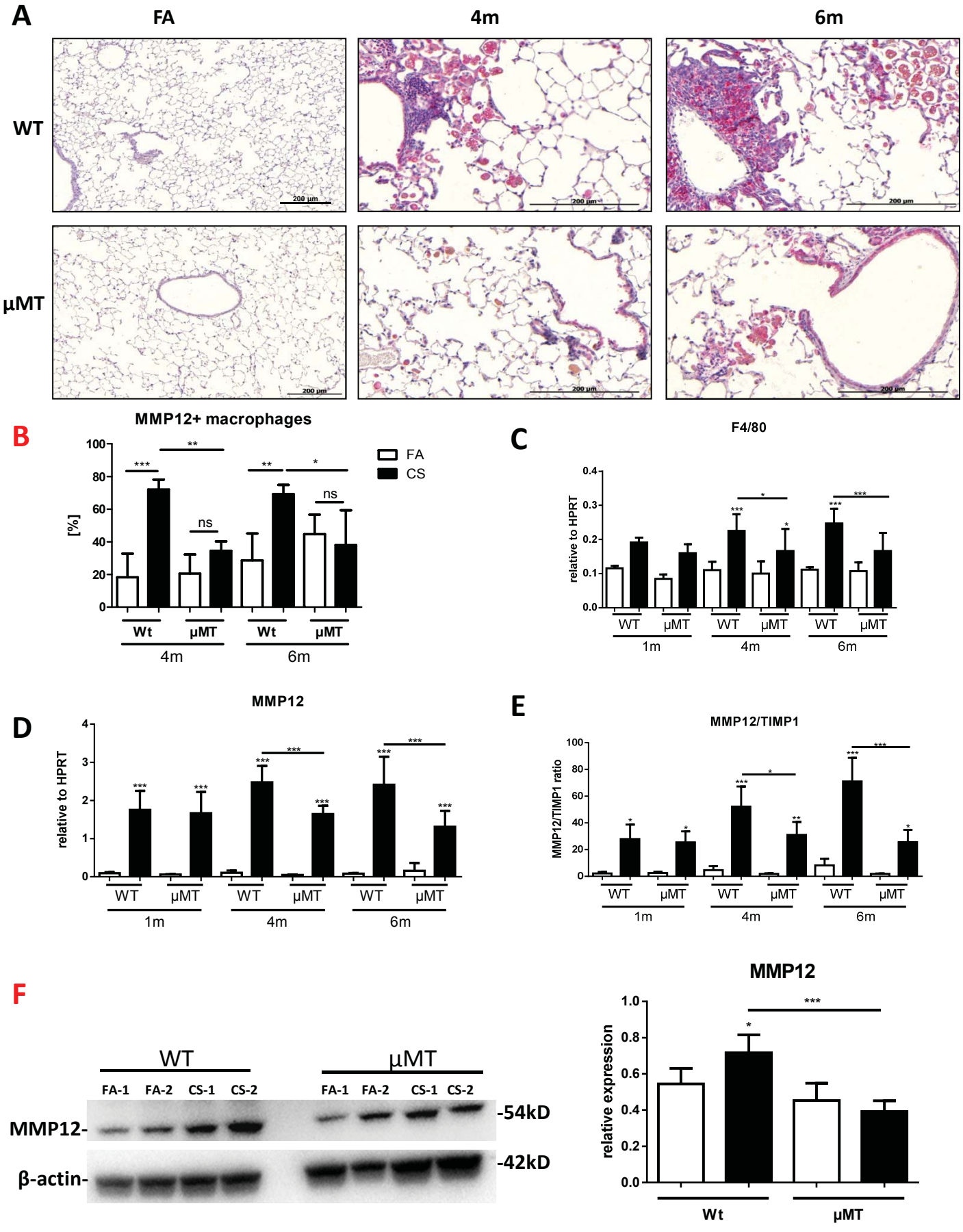
A
FA
4m
6m
WT
µMT
200 µm
B
MMP12+ macrophages
[%]
FA
CS
ns
Wt
µMT
4m
6m
C
F4/80
relative to HPRT
WT
µMT
1m
4m
6m
D
MMP12
relative to HPRT
E
MMP12/TIMP1
MMP12/TIMP1 ratio
F
WT
µMT
FA-1
FA-2
CS-1
CS-2
MMP12-
β-actin-
-54kD
-42kD
MMP12
relative expression

Figure 6

G

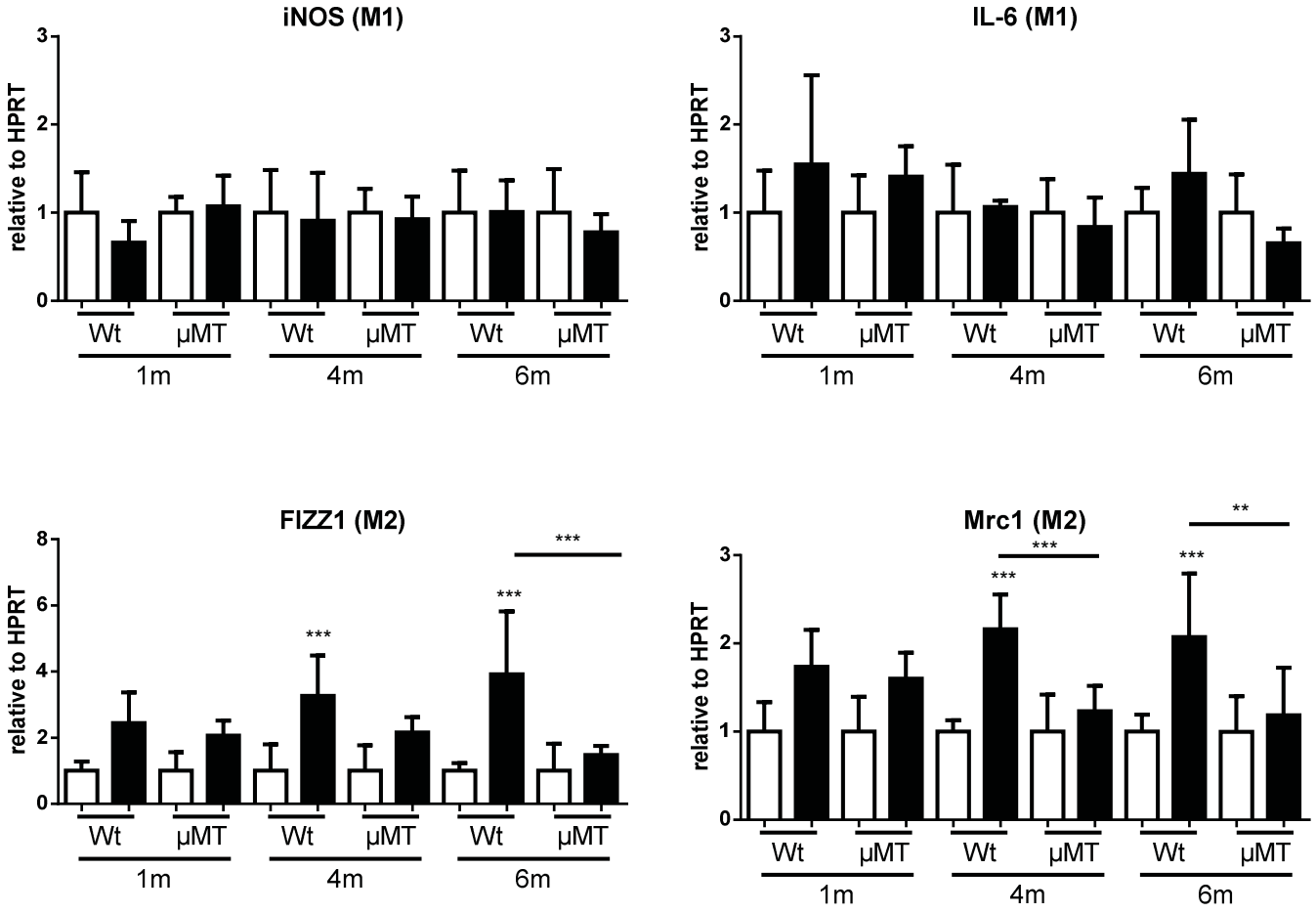

Figure 7- new

A

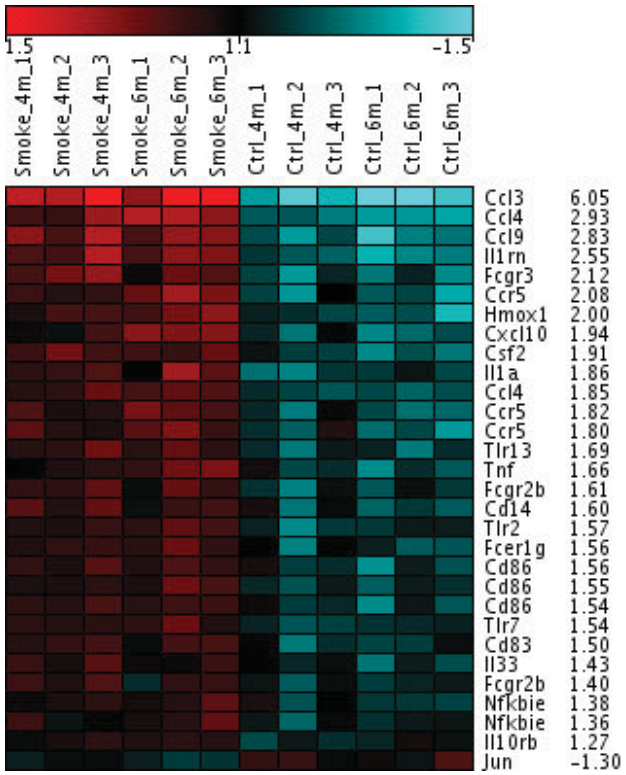

B

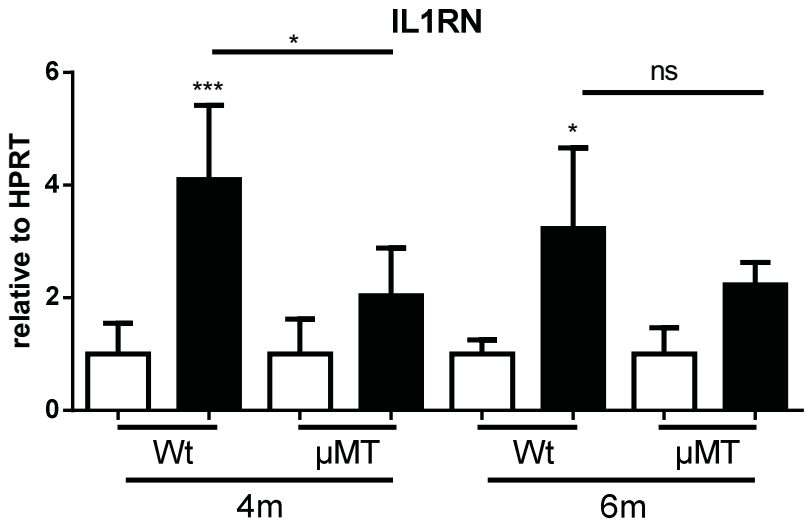

Figure 8

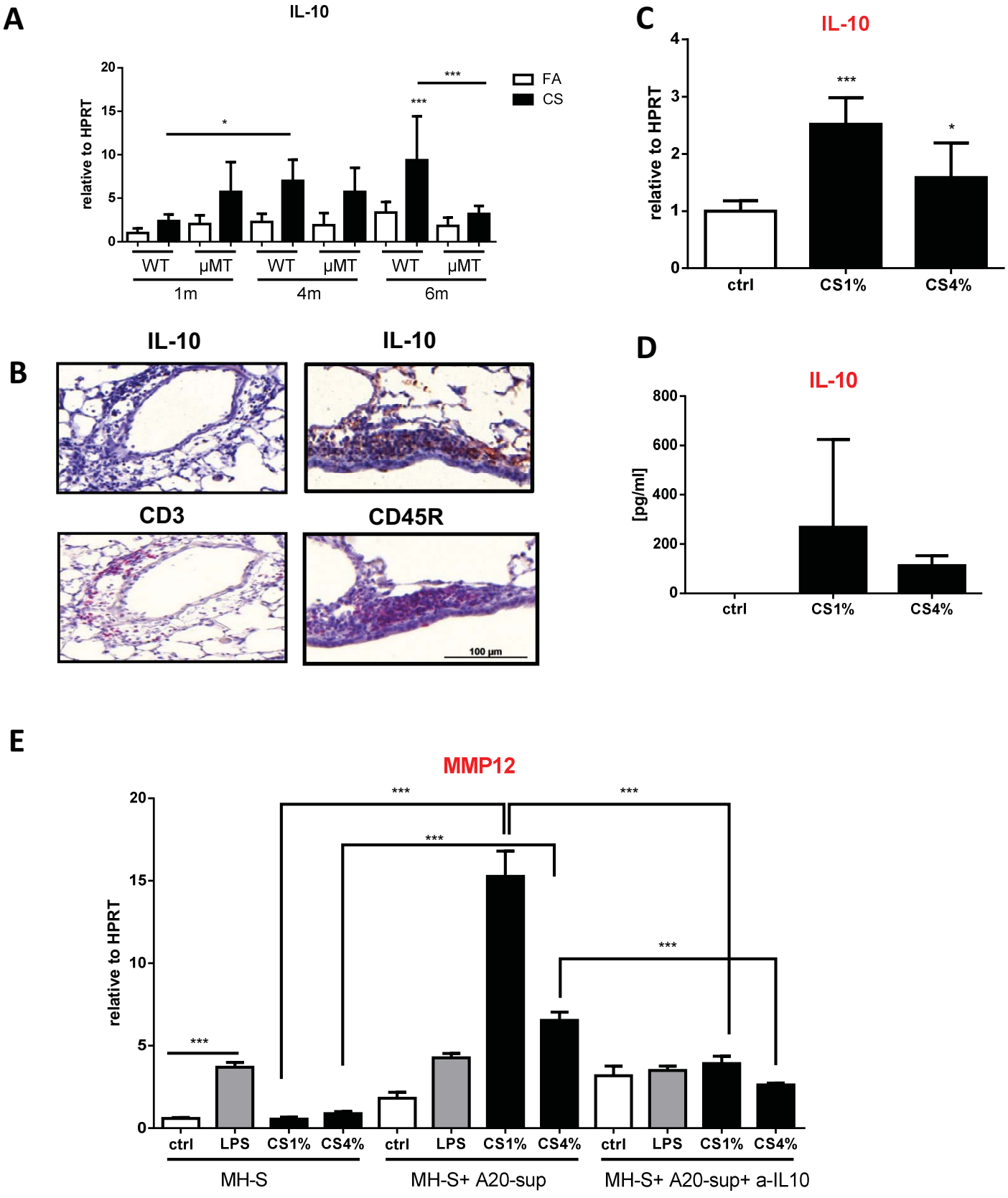
A
IL-10
relative to HPRT
FA
CS
WT
µMT
1m
4m
6m
B
IL-10
IL-10
CD3
CD45R
100 µm
C
IL-10
relative to HPRT
ctrl
CS1%
CS4%
D
IL-10
[pg/ml]
ctrl
CS1%
CS4%
E
MMP12
relative to HPRT
ctrl
LPS
CS1%
CS4%
MH-S
MH-S+ A20-sup
MH-S+ A20-sup+ a-IL10

Table 1. Enriched canonical pathways

Ingenuity Canonical Pathways	-log(p-value)	Ratio	Molecules
Communication between Innate and Adaptive Immune Cells	7.81E+00	1.34E-01	IL1A, CD83, Ccl9, IL33, CXCL10, TLR2, CCL4, IL1RN, FCER1G, TLR7, CD86, CCL3L1/CCL3L3, Tlr13, CSF2, TNF
Role of Hypercytokinemia/hyperchemokinemia in the Pathogenesis of Influenza	5.04E+00	1.74E-01	IL33, CXCL10, IL1A, CCR5, CCL4, CCL2, IL1RN, TNF
IL-10 Signaling	4.95E+00	1.54E-01	IL33, HMOX1, IL1A, CCR5, JUN, FCGR2A, IL1RN, NFKBIE, IL10RB, CD14, FCGR2B, TNF
Atherosclerosis Signaling	4.36E+00	1.08E-01	APOE, IL1A, MMP3, CMA1, MMP13, ALOX12, CCL11, PLA2G7, IL33, ITGB2, PLA2G2D, CCL2, IL1RN, PLA2G4F, TNF
Dendritic Cell Maturation	3.34E+00	7.58E-02	PLCB2, IL1A, TYROBP, FCGR2A, NFKBIE, CD83, FCGR2B, TREM2, IL33, TLR2, IL1RN, FCER1G, CD86, LY75, CSF2, TNF
Crosstalk between Dendritic Cells and Natural Killer Cells	2.65E+00	8.49E-02	CSF2RB, KLRD1, TYROBP, TLR7, CD86, CD83, TREM2, CSF2, TNF
NF-κB Signaling	1.88E+00	7.18E-02	TLR2, IL33, TNIP1, IL1A, TGFBR1, CARD10, IL1RN, NFKBIE, TGFBR3, FCER1G, TLR7, MALT1, TNF
Nicotine Degradation II	1.86E+00	7.06E-02	UGT1A6, CYP4B1, FMO1, CSGALNACT1, UGT1A9, CYP1B1
Systemic Lupus Erythematosus Signaling	1.32E+00	4.31E-02	IL33, IL1A, JUN, FCGR2A, IL1RN, TLR7, FCER1G, CD86, C6, FCGR2B, TNF

Table 1: Lung mRNA expression profiles of four and six months CS-exposed versus FA-exposed mice were determined by microarray analysis using Illumina Mouse Ref-8 v2.0 BeadChip. CS exposure induces a strong activation of ten pathways as analyzed with Ingenuity Pathway software.